Published in final edited form as:

Mol Syst Des Eng. 2017 December 1; 2(5): 624–628. doi:10.1039/c7me00055c.

Modulating the Catalytic Activity of Enzyme-like Nanoparticles Through their Surface Functionalization

Roberto Cao-Milán[a], **Luke D. He**[a], **Spencer Shorkey**[a], **Gulen Y. Tonga**[a], **Li-Sheng Wang**[a], **Xianzhi Zhang**[a], **Imad Uddin**[b], **Riddha Das**[a], **Mine Sulak**[c], and **Vincent M. Rotello**[a]

[a]Department of Chemistry, University of Massachusetts Amherst, 710 North Pleasant Street, Amherst, Massachusetts 01003, USA

[b]Department of Chemistry, Hazara University, Mansehra 21120, Pakistan

[c]School of Applied Science, Pamukkale University, 20600, Çivril, Denizli, Turkey

Abstract

The inclusion of transition metal catalysts into nanoparticle scaffolds permits the creation of catalytic nanosystems (nanozymes) able to imitate the behaviour of natural enzymes. Here we report the fabrication of a family of nanozymes comprised of bioorthogonal ruthenium catalysts inserted in the protective monolayer of gold nanoparticles. By introducing simple modifications to the functional groups at the surface of the nanozymes, we have demonstrated control over the kinetic mechanism of our system. Cationic nanozymes with hydrophobic surface functionalities tend to replicate the classical Michaelis Menten model, while those with polar groups display substrate inhibition behaviour, a key mechanism present in 20 % of natural enzymes. The structural parameters described herein can be used for creating artificial nanosystems that mimic the complexity observed in cell machinery.

Graphical abstract

Bioorthogonal nanozymes displaying different kinetic behaviorscan be created through modifications in their surface functional groups

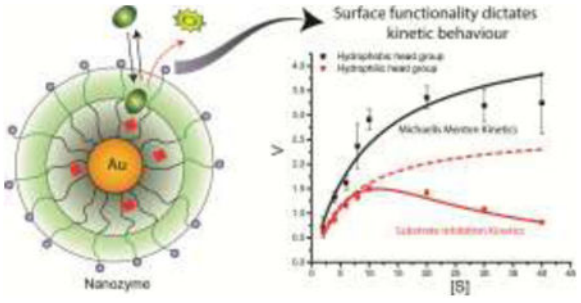

Correspondence to: Vincent M. Rotello.

Electronic Supplementary Information (ESI) available: [details of any supplementary information available should be included here]. See DOI: 10.1039/x0xx00000x

Introduction

Enzymes have evolved to perform a wide variety of transformations,[1] coupling efficiency with a complex suite of regulatory mechanisms.[2] These properties make enzymes important catalysts for synthetic processes, particularly in the area of sustainable chemistry.[3] There are, however, many limitations for enzymatic catalysis ranging from instability to the fact that despite their enormous breadth of mechanisms, there are many reactions that enzymes cannot catalyze.[4]

Bioorthogonal catalysis has opened a promising direction, with transition metal catalysts (TMCs)[5-8] providing access to transformations using chemical processes that are orthogonal to biocatalysis.[9–14] Loading of TMCs into nanomaterial scaffolds provides water solubility and a protective environment for TMCs,[12,14,15] playing a role similar to that of the protein scaffold in enzymatic catalysis. These scaffolds also have the potential to access more complex attributes of enzymatic behaviour, an area that to date has not been well-explored.

In our recent studies we have developed a family of gold nanoparticles (2 nm core, ~7 nm overall diameter) loaded with ruthenium or palladium catalysts, and shown that these "nanozymes" **(NZs)** have catalytic behaviour that can be described as consistent with enzymes, and can be characterized using classical Michaelis-Menten kinetics.[15] We report here the extension of this biomimetic capability to more complex kinetic behaviours. In this study, structural motifs present on the monolayer were used to regulate catalysis, providing systems that feature substrate inhibition, an important mechanism observed in processes that regulate neutrotransmission[16] and DNA methylation,[17] among others.[18] We believe this study constitutes a starting point for the creation of nanozyme-based systems that could eventually replicate the complexity of cellular pathways.

Experimental Section

Materials

All chemicals used were purchased from Fischer Scientific and were used without any previous treatment. Synthesis of nanoparticle scaffolds (NPs) can be found in ESI-2. The substrate (Pro-Rho) was prepared as early reported.[9,15]

Instrumentation

All fluorescence determinations were carried out in a SpectraMax M5 microplate spectrophotometer. The hydrodynamic diameter of **NZs** was measured in a Malvern Zetasizer Nano ZS instrument. The ICP-MS analyses were performed on a Perkin-Elmer NexION 300× ICP mass spectrometer.

Nanozyme preparation

Nanozymes were synthesized following a previous method.[15] A 3 mg/mL solution of the ruthenium catalyst ([Cp*Ru(cod)Cl] in acetone was mixed (1:1 v/v) with an aqueous solution of NPs (20 μM). The acetone was slowly removed by evaporation to favour the encapsulation of the catalyst in the particle monolayer. The mixture was then submitted to filtration (Millex-GP filter; 25 mm PES, pore Size: 0.22μm) to remove the precipitated

catalyst. The nanozyme solutions were subsequently submitted to 5 filtration sessions (Amicon® ultra 4, 10K) and dialysed (Snake Skin® dialysis tubing, 10K) against water (5L, 24h) to remove unbound catalyst. The amount of encapsulated catalyst was measured by ICP-MS by tracking ^{101}Ru relative to ^{197}Au.[15] (ESI-3)

Kinetic studies of nanozymes—The catalytic reactions of the nanozymes were carried out in phosphate buffered saline (PBS, pH 7.4). Nanozymes and substrate stock solutions were mixed in a 96-well plate to provide 100 μL final solution containing 400 nM of **NZs** and **Pro-Rho** at 2, 4, 6, 8, 10, 20, 30 and 40 μM concentrations. Fluorescence evolution of the allyl-carbamate deprotection process was registered immediately after mixing (Ex: 488 nm, Em: 521 nm, Cut-off: 515 nm) for 20 mins at 30 second intervals.

Pro-Rho adsorption on nanoparticles—The experiments for determining the adsorption capacity of each **NPs** for **Pro-Rho** were carried out in PBS (pH 7.4). Each nanoparticle was mixed with stock substrate solutions in a 96-well plate to provide 100 μL final solution containing 400 nM of each nanoparticle and **Pro-Rho** at 2, 4, 6, 8, 14, 16, 18 and 25 μM concentrations. Fluorescence variations of adsorbed **Pro-Rho** was registered (Ex: 488 nm, Em: 521 nm, Cut-off: 515 nm) 5 mins after mixing. Calibration curves and details of the determination can be found in ESI-5.

Results and discussion

Design and synthesis of the nanozymes

Gold nanoparticles with core diameters of 2 nm capped with a monolayer (~2.5 nm thick) were used as the scaffold for the catalysts, with the goal of creating protein-sized systems (Fig. 1a).

The activity of most of enzymes is modulated by the amino acids residues located on their surfaces.[19] Mutations on these amino acids can produce drastic changes in their tertiary structure, thus influencing their kinetic behaviour.[19] With these concepts in mind, the effect of various modifications in the hydrophobicity of nanozyme ligands was explored (Fig. 1b). The structure of the protecting monolayer of the nanozyme platform is ruled by two major interactions: the long hydrophobic segments will interact through attractive Van der Waals forces, while the alkyl ammonium groups generate electrostatic repulsions between these ligands of the monolayer. The balance between these opposing forces should define the degree of compaction of the nanozyme monolayer, and thus, their kinetic behaviour (Fig. 1c). We reasoned that increasing the hydrophobicity of the positively charged head groups would produce a favourable effect towards the compaction of the monolayer, thus impacting the kinetic behaviour of the nanozymes. In this regard, ligands bearing methyl (TTMA), benzyl (DMBzA) and tolyl (DMTolA) substituents were used for constructing the NP scaffolds (Fig. 1b). More hydrophobic ligands were also included in the designs; however, the resulting nanozymes proved insoluble in PBS (see ESI-4).

Figure 1d shows some of the characteristics of our family of nanozymes. It can be observed that the three types of nanozymes used were dispersed in PBS and display sizes comparable with proteins (See also ESI-4).

Kinetic behaviour of nanozymes—The kinetic behaviour of our nanozymes was studied using an allylcarbamate-protected derivative of rhodamine 110 (Pro-Rho), as substrate (Fig. 2a). **Pro-Rho** is a hydrophobic molecule with low fluorescence. After the catalytic deallylation, **Pro-Rho** is transformed into the zwitterionic, strongly fluorescent rhodamine 110 (Fig. 2a).[9] The fluorogenesis of this dye provides a direct way for monitoring reaction kinetics.[9] In addition, the zwitterionic nature of catalysed **Pro-Rho** molecules drastically increases its hydrophilic behaviour, presumably reducing affinity for the hydrophobic pocket of our nanozymes.

Figure 2b shows the kinetic behaviour of the nanozymes in PBS. **DMTolA-NZ** displayed a classical Michaelis-Menten kinetic model, where the rate of conversion tends to asymptote to a steady-state level at high concentration of substrates. Such relationship demonstrates saturation of all nanozyme active sites. The kinetic behaviour of **DMTolA-NZ** can be represented by the classical Michaelis-Menten expression:

$$\frac{\mathbf{V}}{[\mathbf{NZ}]}=\frac{\mathbf{k_{Cat}}[\mathbf{S}]}{\mathbf{K_M}+[\mathbf{S}]} \quad (1)$$

where V is the rate of product formation, [NZ] is the concentration of nanozymes, [S] is concentration of substrate and K_M and k_{Cat} are the Michaelis-Menten and catalytic constants, respectively.

Interestingly, at high concentrations of substrate, **DMBzA-NZ** and **TTMA-NZ** tend to reduce the conversion rate of substrate. This type of catalytic behaviour is known as substrate inhibition and is also present in a large group of natural enzymes.[18] In such cases, at high concentrations, substrate can bind inactive pockets of the enzyme, producing antagonistic effects. [16-18] In the case of the NZs, any hydrophobic pocket without the ruthenium catalyst can be, in principle, able to bind substrate, producing the abovementioned allosteric attenuation of catalysis (Fig. 2c right)

The behaviour of **DMBzA-NZ** and **TTMA-NZ** was modelled by the equation used for describing substrate inhibition mechanism:[16]

$$\frac{\mathbf{V}}{[\mathbf{NZ}]}=\frac{\mathbf{k_{Cat}}[\mathbf{S}]}{\mathbf{K_M}+[\mathbf{S}]+\frac{[\mathbf{S}]^2}{\mathbf{K_i}}} \quad (2)$$

In equation 2, K_i represents the dissociation constant of substrate binding the allosteric sites (Fig. 2c right) and producing a 50% reduction of catalytic activity (for comparison, see in figure 2a simulated curves for **TTMA-NZ** and **DMBzA-NZ** without substrate inhibition effect).

With the increase in the hydrophobicity of the substituent of the alkyl ammonium head groups, the value of increases K_i until no additional substrate can influence the activity of

nanozymes, as in the case of **DMTolA-NZ** (Fig. 2d. Note also that for large Ki values equation 2 tends to equation 1). An increase in the hydrophobicity of the positively charged head group also tended to increase the value of K_M. However, variations on K_M are not as pronounced as in K_i.

The observed kinetic results suggest that increased compaction of the monolayer, driven by an increasingly hydrophobic ligand, induces nanozyme behaviour to follow the classical Michaelis-Menten model. To test this hypothesis a nanozyme bearing an uncharged head group was synthesized and studied (See ESI 7). In this design, ligands in the protecting monolayer of the nanozyme do not experience electrostatic repulsion; thus, attractive Van der Waals forces should dominate. ESI 7 shows that TEGOH-NZs displayed classical Michaelis-Menten behaviour. These results are consistent with our understanding of the effect of monolayer compaction on the kinetic mechanism of the nanozyme.

Substrate adsorption experiments—The observed trend for magnitudes of both K_M and K_i suggests that the affinity of substrate for nanozymes tends to decrease with increasing hydrophobicity of the alkyl ammonium head group. Therefore, an experiment to explore the capacity of our **NP** scaffolds to adsorb substrate was carried out. Adsorption capacity of **NPs** was determined in PBS by monitoring the quenching effect of gold particles on the residual fluorescence of adsorbed **Pro-Rho**. It should be noted that adsorption experiments are carried out in equilibrium conditions; thus, only the **NP** scaffolds (without the ruthenium catalyst) can be used.

Figure 3a shows the number of molecules of **Pro-Rho** adsorbed in the monolayer of each of our **NPs** at different concentrations of this substrate. Increasing the hydrophobicity of the alkyl ammonium group was observed to reduce the adsorption capacity of the corresponding **NP**. In addition, **Pro-Rho** adsorption curves shift to sigmoidal shapes for the **NPs** bearing the most hydrophobic surface functionalities (Fig. 3a). This sigmoidal behaviour (as **DMTolA-NP)** indicates that the inclusion of **Pro-Rho** into the monolayer of **NPs** is not favoured at low concentrations of the substrate. However, insertion of the first few molecules into this monolayer contributes to subsequent adsorption of the substrate via a cooperative effect (Fig. 3b). In the case of **TTMA-NPs**, the linear behaviour suggests that the amount of adsorbed **Pro-Rho** is only dependent on the concentration of substrate in solution (Fig. 3c).

The trend observed for **Pro-Rho** adsorption could be caused by different levels of compaction of the monolayer of our **NP** scaffolds, with **DMTolA-NP** displaying the most compact one and **TTMA-NP** the less. To confirm this assumption, the same adsorption experiment was carried out in deionized water. Under low ionic strength conditions, the monolayer of our NP scaffolds should acquire a lower compaction degree.[20,21] All NPs scaffolds displayed increased substrate adsorption capacity in deionized water than PBS (see ESI-4). These results suggest that the more expanded the monolayer of our **NPs** the greater their capacity to associate substrates (see ESI-5).

The results obtained by these adsorption experiments with our **NPs** scaffolds shed some light on how **DMTolA-NZ** displays Michaelis-Menten kinetic behaviour while **DMBzA-NZ** and **TTMA-NZ** exhibit substrate inhibition. We hypothesized that the higher compaction of

the monolayer of **DMTolA-NZ** reduces the affinity for **Pro-Rho**; thus, decreases the possibility of insertion of substrate in allosteric sites. However, in the case of **DMBzA-NZ** and **TTMA-NZ**, with a more opened monolayer, at high concentrations **Pro-Rho** can bind both active and allosteric sites. Our next steps will focus on answering questions regarding the key structural parameters that modulate the efficiency and selectivity of these bioorthogonal nanozymes.

Conclusion

In conclusion, we have demonstrated the construction of bioorthogonal nanozymes featuring different kinetic behaviours present in natural enzymes. The kinetic mechanism of nanozymes was observed to be strongly influenced by their surface functionalities. The ability to fabricate bioorthogonal nanozymes featuring sophisticated enzymatic behaviours is essential for developing a platform of nanodevices able to modulate complex cell bioprocesses through abiotic catalytic reactions, with envisaged applications in both fundamental science and biomedical procedures.

Supplementary Material

Refer to Web version on PubMed Central for supplementary material.

Acknowledgments

This research was supported by the NIH (EB022641) and the NSF (CHE-1506725). M. S. acknowledges TÜBİTAK for the fellowship 1059B191501588.

References

1. Bisswanger, H. Enzyme Kinetics: Principles and Methods. 2nd. Wiley-VCH Verlag GmbH & Co.; KGaA, Weinheim, Germany: 2008. p. 124-193.ch. 2.6-2.12
2. Evans MJ, Cravatt BF. Chem Rev. 2006; 106:3279–3301. [PubMed: 16895328]
3. Husain Q. Crit Rev Biotechnol. 2006; 26:201–221. [PubMed: 17095432]
4. a) Carell T, Vrabel M. Top Curr Chem. 2016; 374:9.b) Lin Y, Ren J, Qu X. Acc Chem Res. 2014; 47:1097–105. [PubMed: 24437921]
5. Sletten EM, Bertozzi CR. Acc Chem Res. 2011; 44:666–676. [PubMed: 21838330]
6. Saxon E, Bertozzi CR. Science. 2000; 287:2007–2010. [PubMed: 10720325]
7. Sasmal PK, Streu CN, Meggers E. Chem Commun. 2013; 49:1581–1587.
8. Unciti-Broceta A, Johansson EMV, Yusop RM, Sánchez-Martín RM, Bradley M. Nat Protocols. 2012; 7:1207–1218. [PubMed: 22653159]
9. Streu C, Meggers E. Angewandte Chemie Int Ed. 2006; 45:5645–5648.
10. Do JH, Kim HN, Yoon J, Kim JS, Kim HJ. Org Lett. 2010; 12:932–934. [PubMed: 20112946]
11. Sasmal PK, Carregal-Romero S, Han AA, Streu CN, Lin Z, Namikawa K, Elliott SL, Köster RW, Parak WJ, Meggers E. ChemBioChem. 2012; 13:1116–1120. [PubMed: 22514188]
12. Yusop RM, Unciti-Broceta A, Johansson EMV, Sánchez-Martín RM, Bradley M. Nat Chem. 2011; 3:239–243. [PubMed: 21336331]
13. Völker T, Meggers E. Curr Opin Chem Bio. 2015; 25:48–54. [PubMed: 25561021]
14. Weiss JT, Dawson JC, Macleod KG, Rybski W, Fraser C, Torres-Sánchez C, Patton EE, Bradley M, Carragher NO, Unciti-Broceta A. Nat Commun. 2014; 5:3277. [PubMed: 24522696]
15. Tonga GY, Jeong Y, Duncan B, Mizuhara T, Mout R, Das R, Kim ST, Yeh YC, Yan B, Hou S, Rotello VM. Nat Chem. 2015; 7:597–603. [PubMed: 26100809]

16. Winge I, Mckinney JA, Ying M, D'Santos CS, Kleppe R, Knappskog PM, Haavik J. Biochem J. 2008; 410:195–204. [PubMed: 17973628]
17. Jones PA, Takai D. Science. 2001; 293:1068–1070. [PubMed: 11498573]
18. Reed MC, Lieb A, Nijhout HF. Bioessays. 2010; 32:422–429. [PubMed: 20414900]
19. Yu F, Cangelosi VM, Zastrow ML, Tegoni M, Plegaria JS, Tebo AG, Mocny CS, Ruckthong L, Qayyum H, Pecoraro VL. Chem Rev. 2014; 114:3495–3578. [PubMed: 24661096]
20. Volkert AA, Subramaniam V, Ivanov MR, Goodman AM, Haes AJ. ACS Nano. 2011; 5:4570–4580. [PubMed: 21524135]
21. Mout R, Tonga GY, Wang LS, Ray M, Roy T, Rotello VM. ACS Nano. 2017; 11:3456–3462. [PubMed: 28225593]

Design, System, Application

Nanocatalysis is an important tool for sustainable chemistry and biology. Maximizing the efficiency of nanocatalysts is crucial, however little work has been done towards developing nanosystems able to mimic the sophisticated kinetic behaviors of natural enzymes. Here we report the construction of nanocatalysts comprised of bioorthogonal ruthenium catalysts inserted into the protecting monolayer of gold nanoparticles. By introducing simple modifications in their surface functional groups, these “nanozymes” could be engineered to display kinetic behaviors observed in natural enzymes, including both “simple” classical Michaelis-Menten as well as substrate inhibition mechanisms. These studies provide initial steps toward understanding the structural parameters that modulate the catalytic behavior of nanozymes required for developing new nanodevices with controlled kinetic characteristics.

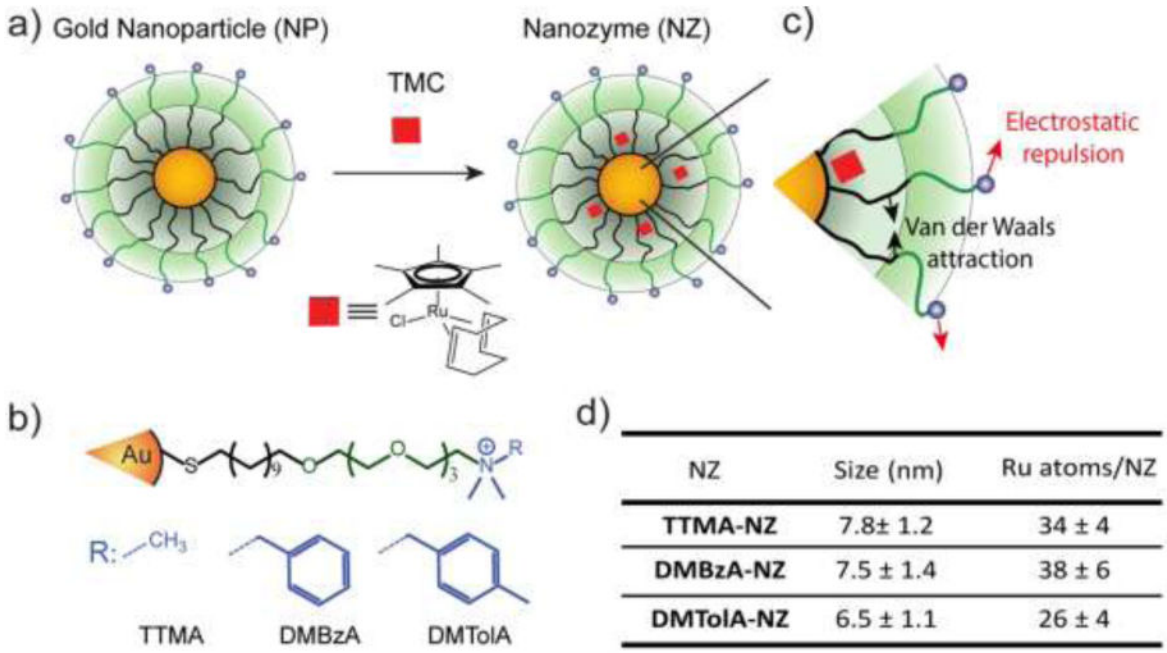

NZ	Size (nm)	Ru atoms/NZ
TTMA-NZ	7.8± 1.2	34 ± 4
DMBzA-NZ	7.5 ± 1.4	38 ± 6
DMTolA-NZ	6.5 ± 1.1	26 ± 4

Figure 1.

Structure of nanozymes. a) Encapsulation of TMCs in the hydrophobic pocket of gold nanoparticles. b) Structure of the nanoparticle scaffolds for generating cationic nanozymes with different hydrophobic surface functional groups. c) Schematic representation of the interacting forces among the ligands in the monolayer. Black arrows represent Van der Waals attraction. Red arrows represent repulsive electrostatic interaction. d) Table containing the size (determined via dynamic light scattering) and the amount of Ru catalyst per nanozyme. Mean values ± standard deviation, N = 3

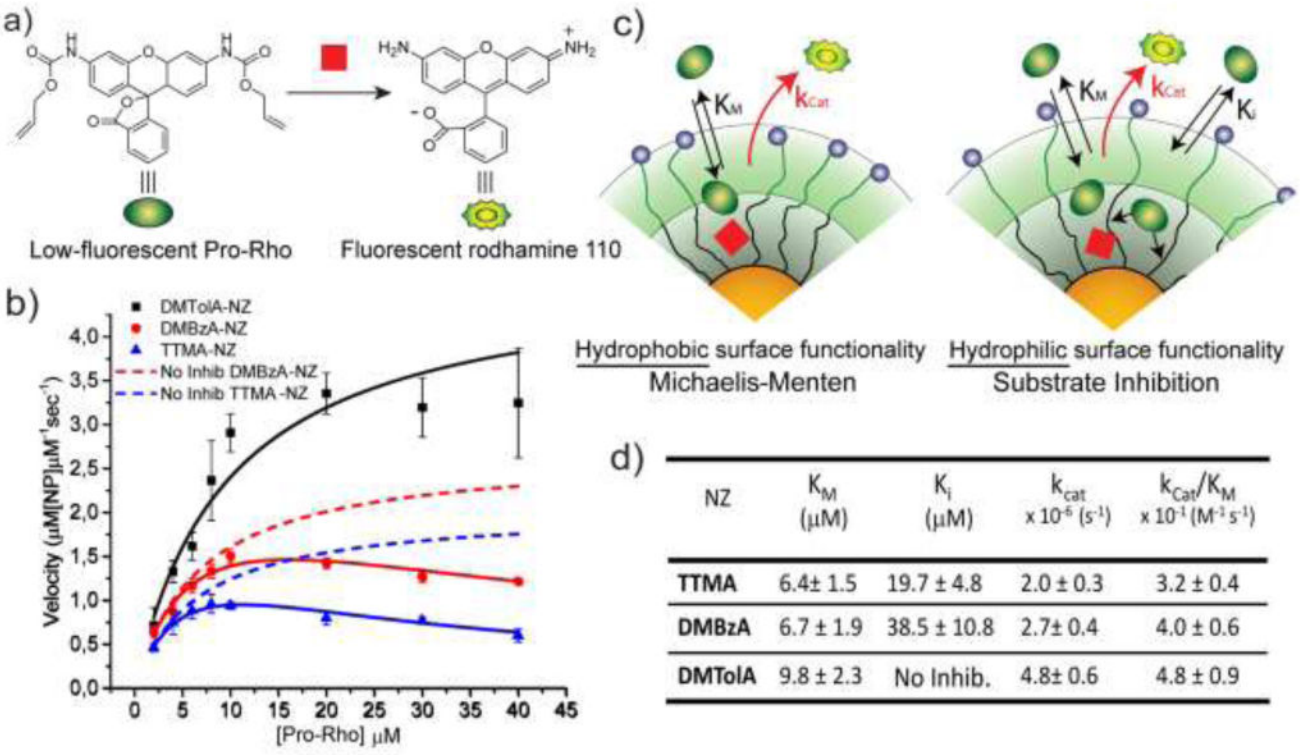

d)

NZ	K_M (μM)	K_i (μM)	k_{cat} x 10^{-6} (s^{-1})	k_{Cat}/K_M x 10^{-1} ($M^{-1}s^{-1}$)
TTMA	6.4± 1.5	19.7 ± 4.8	2.0 ± 0.3	3.2 ± 0.4
DMBzA	6.7 ± 1.9	38.5 ± 10.8	2.7± 0.4	4.0 ± 0.6
DMTolA	9.8 ± 2.3	No Inhib.	4.8± 0.6	4.8 ± 0.9

Figure 2.

Kinetic study of nanozymes. a) Schematic representation of the activation of allyl carbamate protected rhodamine 110 (Pro-Rho). B) Nanozyme kinetics are shown as a function of substrate concentration. Solid lines are the regression curves corresponding to each mechanism. Dashed lines correspond to simulated kinetic curves for **TTMA-NZ** and **DMBzA-NZ** without substrate inhibition effect. c) Schematic representations of two possible kinetic behaviours of nanozymes. Left, nanozymes with monolayers bearing hydrophobic quaternary alkyl ammonium groups display the Michaelis-Menten mechanism. Right, nanozymes bearing hydrophilic quaternary alkyl ammonium groups display a substrate inhibition mechanism. d) Kinetic parameters for each nanozyme. Mean values ± standard deviation, N = 3

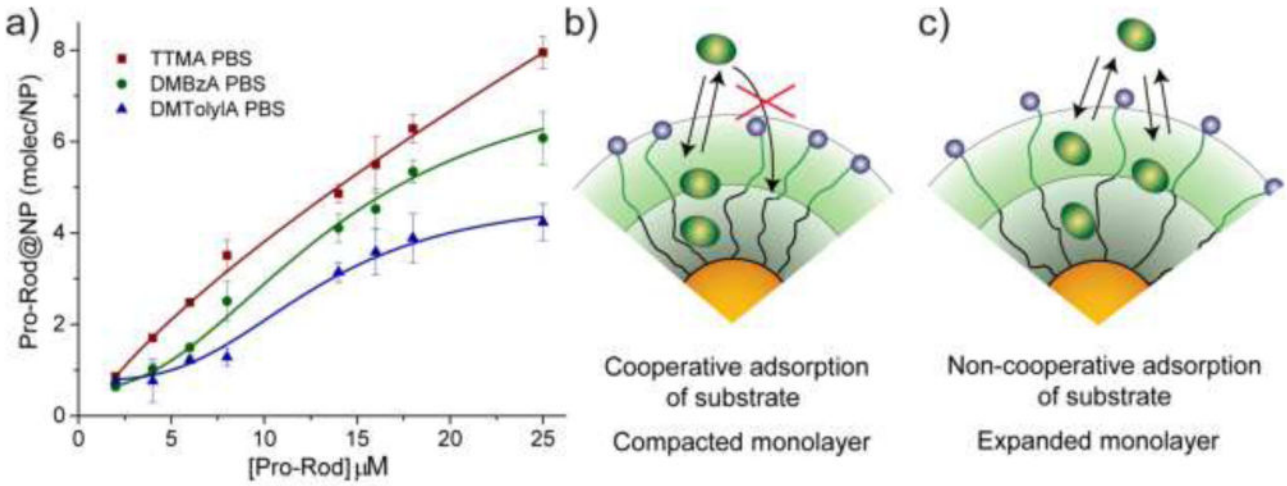

Figure 3.

Adsorption of **Pro-Rho** on the nanoparticle scaffolds used. a) Adsorption curves of **Pro-Rho** on each **NP** in PBS. Adsorbed **Pro-Rho** molecules on the **NPs** were plotted as function of **Pro-Rho** concentration. b) Schematic representations of the cooperative adsorption mechanism observed in **DMTolA-NP** featuring compact monolayer: The first adsorbed molecules favour the further adsorption of substrate c) Non-cooperative adsorption of substrate on **TTMA-NP**. The adsorption of **Pro-Rho** molecules is only dependent on its concentration in solution. Adsorbed molecules do not influence the further adsorption of substrate. Mean values ± standard deviation, N = 3